Measurement of the quasi-elastic axial vector mass in neutrino-oxygen interactions

Richard Gran,* Eun Ju Jeon,† and K2K collaboration
High Energy Accelerator Research Organization (KEK)
Tsukuba 305-0801, Japan
Replace these with the full author list later.
(Dated: August 23, 2005)

The weak nucleon axial-vector form factor for quasi-elastic interactions is determined using neutrino interaction data from the K2K Scintillating Fiber detector in the neutrino beam at KEK. More than 12,000 events are analyzed, of which half are charged-current quasi-elastic interactions $\nu_\mu n \to \mu^- p$ occurring primarily in oxygen nuclei. By assuming the form factor is approximately a dipole with one parameter, the axial vector mass M_A, we fit to the shape of the distribution of the square of the momentum transfer from the nucleon to the nucleus. Our best fit result for $M_A = 1.16 \pm 0.12$ GeV. This analysis includes updated vector form factors from recent electron scattering experiments and a discussion of the effects of the nucleon momentum on the shape of the fitted distributions.

PACS numbers: 13.15.+g; 23.40.Bw; 25.30.Pt

I. INTRODUCTION

The structure of the nucleon, as measured both by electrons and neutrinos, has been a subject of experimental study for decades. The discovery of neutrino oscillation and the availability of high precision electron scattering measurements have renewed interest in the study of neutrino interactions on nuclei. Neutrinos offer unique information about the nucleon and the nucleus. There are many experimental neutrino programs now running, under construction, or being planned for the near future, all of which use nuclear targets such as oxygen, carbon, aluminum, argon, or iron. Likewise, there has been significant progress in the calculation of cross sections, backgrounds, and nuclear corrections. Improvement of these models, supported by neutrino data, will be important for the upcoming precision neutrino oscillation studies.

In this study we analyze distributions of the square of the four-momentum transfer $Q^2 = -q^2 = -(p_\mu - p_\nu)^2$ reconstructed from neutrino-oxygen interactions, where p_μ and p_ν are the momenta for the outgoing muon and incident neutrino. Using data from the Scintillating Fiber (SciFi) detector in the KEK accelerator to Kamioka (K2K) neutrino beam, we fit for the value of the axial vector mass M_A, the single parameter in the axial vector form factor (assuming a dipole form) for quasi-elastic (QE) interactions. For QE interactions, this parameter is obtained only from neutrino-nucleus scattering experiments. This is the first such measurement for oxygen nuclei, and we include a discussion of the effects of the oxygen nucleus and nucleon momentum distribution on the shape of the Q^2 distribution.

*Now at University of Minnesota, Duluth
†Now at Seoul National University

II. CROSS SECTION AND FORM FACTOR EXPRESSIONS

A. Quasi-elastic cross section

The differential cross section $d\sigma/dq^2$ for neutrino quasi-elastic scattering ($\nu_\mu n \to \mu^- p$) is described in terms of the vector, axial-vector, and pseudo-scalar form factors. The differential cross section[1] is written as:

$$\frac{d\sigma^\nu}{dq^2} = \frac{M^2 G_F^2 \cos^2\theta_c}{8\pi E_\nu^2} \times \left[A(q^2) - B(q^2)\frac{s-u}{M^2} + C(q^2)\frac{(s-u)^2}{M^4} \right] \quad (1)$$

where, s and u are Mandelstam variables, (s-u) = $4ME_\nu + q^2 - m^2$, m is the outgoing lepton mass, M is the target nucleon mass, and E_ν is the neutrino energy. $A(q^2)$, $B(q^2)$, and $C(q^2)$ are:

$$\begin{aligned} A(q^2) &= \frac{m^2 - q^2}{4M^2}\left[(4 - \frac{q^2}{M^2})|F_A|^2 \right. \\ &\quad -(4 + \frac{q^2}{M^2})|F_V^1|^2 - \frac{q^2}{M^2}|\xi F_V^2|^2(1 + \frac{q^2}{4M^2}) \\ &\quad \left. -\frac{4q^2 F_V^1 \xi F_V^2}{M^2} - \frac{m^2}{M^2}((F_V^1 + \xi F_V^2)^2 + |F_A|^2) \right], \\ B(q^2) &= \frac{q^2}{M^2}((F_V^1 + \xi F_V^2)F_A), \\ C(q^2) &= \frac{1}{4}\left(|F_A|^2 + |F_V^1|^2 - \frac{q^2}{4M^2}|\xi F_V^2|^2 \right). \end{aligned} \quad (2)$$

In these expressions, the pseudo-scalar form factor F_P is negligible for muon neutrino scattering away from the muon production threshold and is not included. F_A is the axial vector form factor we will extract from the data. $F_V^1(q^2)$ and $F_V^2(q^2)$ are the Dirac electromagnetic isovector form factor and the Pauli electromagnetic isovector form factor, respectively. These formulas also assume the

conserved vector current (CVC) hypothesis, which allows us to write F_V^1 and F_V^2 in terms of the well measured Sachs form factors G_E^P, G_E^N, G_M^P, and G_M^N:

$$\begin{aligned} F_V^1(q^2) &= (1-\frac{q^2}{4M^2})^{-1}\Big[(G_E^P(q^2)-G_E^N(q^2)) \\ &\quad -\frac{q^2}{4M^2}(G_M^P(q^2)-G_M^N(q^2))\Big], \\ \xi F_V^2(q^2) &= (1-\frac{q^2}{4M^2})^{-1}\left[(G_M^P(q^2)-G_M^N(q^2))\right. \\ &\quad \left.-(G_E^P(q^2)-G_E^N(q^2))\right]. \end{aligned} \tag{3}$$

In this paper we use the updated measurements of the Sachs form factors from [2, 3]. These new form factors have a significant effect on the extraction of F_A, compared to the previous dipole approximations. For the range of Q^2 of interest in this experiment, the updated values differ from the old form factors by up to ± 10%. We present results with both the new and the old form factors in this paper.

We approximate the axial vector form factor F_A as a dipole

$$F_A(q^2) = -\frac{1.2720}{\left(1-(q^2/M_A^2)\right)^2}, \tag{4}$$

which has a single free parameter, the axial vector mass. Previous studies show that this approximation is reasonable [4–6]. The constant $F_A(q^2{=}0) = g_A/g_V = 1.2720{\pm}0.0018$ is determined from neutron decay measurments[7]. Because the Sachs form factors and other constants are precisely measured, the single parameter M_A can be determined from quasi-elastic neutrino interaction data.

B. Other cross sections

For this analysis, approximately half of the data comes from non quasi-elastic interactions, mostly single pion events from the production and decay of the N and Δ baryon resonances within the nucleus. This background is described by the NEUT neutrino interaction Monte Carlo simulation [8] used by the K2K and Super-Kamiokande experiments. The resonance single pion events are from the model of Rein and Sehgal[9]. Deep inelastic scattering is from GRV94[10] for the nuclear structure functions with a correction described by Bodek and Yang[11]. The software PYTHIA/JetSet [reference] is used to generate these events. This analysis takes the charged current coherent pion cross section to be zero following [12], and include neutral current coherent pion interactions as in Rein and Sehgal[13] with modifications following Marteau[14, 15], which has been used in previous K2K publications.

C. Nuclear Effects

Equation 1 is the differential cross section for the *free* nucleon, and must be modified to account for the effects of a nucleon bound in a nucleus. In the SciFi detector, the fiducial mass fractions are 0.690 H_2O, 0.217 Al, 0.094 HC, with an error of ±0.004. Our neutrino interaction Monte Carlo treats the entire fiducial mass as if it was made of H_2O; for targets other than a proton in Hydrogen, we use a uniform Fermi gas model with k_f = 225 GeV/c for the nucleon momentum and an effective binding energy of -27 MeV, which is appropriate for oxygen. The primary effect of this nucleon momentum distribution on the quasi-elastic events is an overall suppression of ∼2% for the entire Q^2 distribution and a significant suppression at low Q^2 due to Pauli blocking. The Fermi gas model is also applied to the non quasi-elastic interactions.

In addition to cross section effects, there are final-state interactions. The nucleus will cause reinteraction or absorption of secondary pions and recoil protons. This will affect the observed distribution of the number of tracks. The resulting μ^- is also affected by the Coulomb interaction as it leaves the nucleus, losing approximately 3 MeV, though this effect is implicitly included in the Fermi gas parameters. The above nuclear effects are discussed quantitatively in the results section.

III. EXPERIMENT

A. The beam and detectors

The KEK to Kamioka (K2K)[16–18] experiment is a long baseline neutrino oscillation measurement in which a beam of neutrinos is sent from the KEK accelerator in Tsukuba, Japan to the underground Super-Kamiokande detector[19]. The neutrinos pass through a set of near neutrino detectors 300 meters from the target, after which they travel 250 km to Super-Kamiokande. The analysis in this paper considers only neutrino interactions detected in the Scintillating Fiber (SciFi) detector, one of the near detectors.

The wide-band neutrino beam at KEK is produced when 12 GeV protons hit an aluminum target. Two magnetic horns focus positively charged pions and kaons into a 200 meter long decay pipe, where they decay to μ^+ and ν_μ. The μ^+ are absorbed by approximately 100 meters of earth between the beam dump and the near detector hall. The resulting neutrino energy is between 0.3 and 5 GeV and peaks at 1.2 GeV. The contamination in this beam includes 1.3% ν_e and 0.5% anti-ν_μ. There are also a small number of muons which need to be vetoed; they come from in-time muon generation in the rock and upstream material in the detector hall and a negligible number of muons surviving from the beam dump and decay pipe. These are rejected by an upstream scintillator veto system. Cosmic rays are rejected by a beam timing

requirement, and are also negligible.

The near detector hall of the K2K experiment contains several detectors, shown in Fig. 1. The first detector in the beam is the one-kiloton water Cerenkov detector. This study uses data from the SciFi detector, which is described in detail below. Following SciFi is the location of the lead glass detector which was used to measure the ν_e contamination in the beam. The lead glass detector was removed in 2002 and in its place was a prototype for a plastic scintillator (SciBar) detector. Then in 2003, the full SciBar detector [20] was installed, though data from this last running period is not used in the present analysis. Finally, there is a muon range detector (MRD) [21] which is used to estimate the momentum of the muons from charged current neutrino interactions which escape the SciFi detector. The MRD is also used to monitor the stability of the neutrino beam.

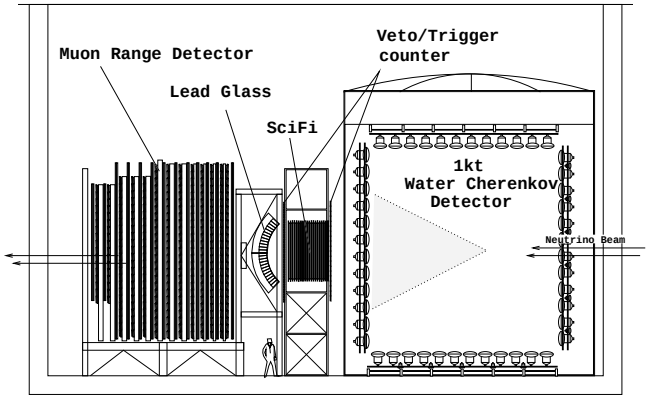

FIG. 1: The arrangement of the near neutrino detectors at KEK (left). The beam comes in from the right and continues to Super-Kamiokande, 250 km away to the left.

The prediction for the shape of the neutrino energy spectrum of the K2K beam has significant uncertainty, up to 20% at higher energies. This prediction uses a Sanford-Wang parameterization of hadron production data and is verified using pion monitors downstream from the target[16]. For the oscillation analysis, this energy spectrum is measured[18] using data from the near detectors. The energy spectrum analysis is a simultaneous fit to the muon momentum and muon angle distributions from charged current interactions in the one-kiloton water Cerenkov detector, the SciFi detector, and the SciBar detector. The free parameters in this fit are a scale factor for the flux in eight energy regions, a scale factor for non quasi-elastic events, and many sytematic error parameters specific to each detector. In this section (Sec. III) of this paper, the above procedure defines the baseline Monte Carlo prediction for the SciFi detector data, prior to any fitting for the axial-vector mass. This default MC simulation also uses zero charged current coherent pion, $M_A^{QE} = 1.1$ GeV and $M_A^{1\pi} = 1.1$ GeV. The resonance single-pion cross section also involves its own axial-vector term with its own M_A. The analysis described in Sec. IV and V is mostly independent from the energy spectrum analysis, but uses a similar strategy.

B. The SciFi detector

The SciFi detector [22, 23] consists of scintillating fiber tracking layers between aluminum tanks filled with water. A schematic diagram is included in Fig. 2. There are a total of twenty 240 cm x 240 cm wide tracking layers, each of which consists of fibers oriented to give the particle location in the horizontal and vertical direction. These fibers are glued, one layer on each side, to a honeycomb panel which is 260 cm square. The distance between two tracking layers is 9 cm. Between the first and the twentieth layer are nineteen layers of aluminum tanks whose walls are 0.18 cm thick with an interior thickness 6 cm filled with water.

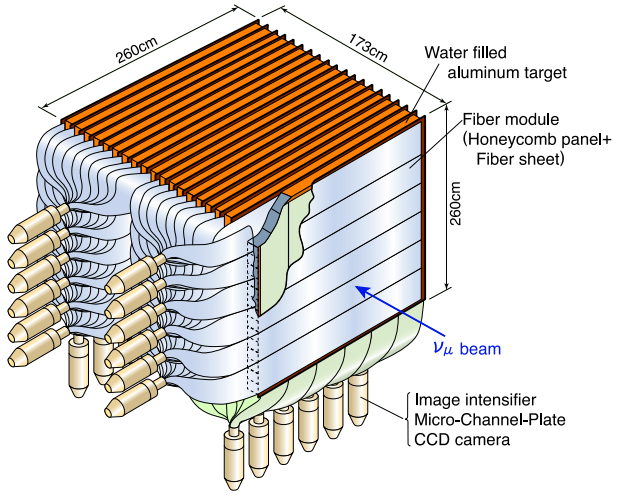

FIG. 2: A schematic diagram of the SciFi detector.

The scintillating fibers have a diameter of 0.7 mm and are read out by coupling them to image intensifier tubes and CCD cameras. The image intensifier preserves the position information of the original photo-electron. At the final stage, the light is recorded by a CCD camera. A total of 24 of these are used to read out 274,080 scintillating fibers. To reconstruct which fibers were hit, a one-to-one correspondence between the fibers and the position of pixels on the CCD camera is obtained from periodic calibration using an electro-luminescent plate.

To select charged-current events for this analysis, we require at least one track start in the SciFi fiducial vol-

ume and extend to the MRD. The fiducial volume includes the first through 17th tanks of water, and the reconstructed vertex must be within 110 cm from the center of SciFi in horizontal and vertical directions, and has a mass of 4900 kg. This requirement means that all events selected for this analysis have hits in at least three tracking layers of SciFi. There are also upstream and downstream scintillator hodoscopes which are read out by photo-multiplier tubes; we require a matching hit downstream and no hit upstream. Starting in 2002, there are additional scintillator on the top and side of SciFi, but these are not used in this analysis.

Tracks are reconstructed in the horizontal and vertical projections separately and then matched. The efficiency for reconstructing muon tracks with hits in three SciFi tracking layers is ∼70%, and rises to nearly 100% for tracks that penetrate five or more layers. Second tracks are required to produce hits in at least three SciFi layers, but there is no restriction on the maximum length. When two tracks reach the MRD, the longest, most penetrating track is assumed to be the muon. Approximately 2% of these longest tracks are not the muon track, and another 0.5% of events were from neutral current interactions which had no muon at all, which we have estimated using the MC.

Prior to 2002, all muons from SciFi are required to pass through and produce hits in segments of the lead glass detector, and these segments must match the location of the reconstructed track seen in SciFi and the MRD. On average, they deposit around 0.4 GeV of energy in the lead glass, though only path length, and not pulse size, is used to estimate the energy loss in this case. After 2002, muons traveling through the SciBar prototype lose around 0.023 GeV of energy, though we do not require the track to pass through this detector. Muons traveling through many layers in SciFi deposit up to 0.3 GeV of energy.

The Muon Range Detector is made of alternating layers of drift tubes and iron plates; the first detection layer is upstream of the first piece of iron. The first four layers have a thickness equivalent to about 0.14 GeV of energy loss each, and the remaining layers are twice as thick. The muon momentum can then be estimated by calculating its range from the interaction vertex.

C. Data samples

The data for this analysis are obtained from two running periods between November 1999 and June 2003. The primary distinction between them is the configuration of the Super-Kamiokande detector, though there were simultaneous changes in the near detector configuration. We refer to the first as the "K2K-I" period; muons from neutrino interactions in SciFi pass through the lead glass detector on their way to the MRD. For these data, we accept muons which penetrate as little as one MRD detection layer, which corresponds to a muon momentum threshold of 675 MeV/c. The second running period is called "K2K-IIa" and has the prototype for the plastic scintillator detector SciBar [20] in place of the lead glass. For K2K-IIa, we require that the muons produce hits in the first *two* layers of the MRD, which gives a threshold of 550 MeV/c, in order to reduce the contamination from pions reaching the MRD. Data from the continuation of the K2K-II period are not used in this analysis. In all cases, we require the muon not exit the MRD, which results in a maximum muon momentum of 3.5 GeV/c.

This analysis uses only one-track and two-track events. Since quasi-elastic interactions will not produce such events, the 3% of events with three or more reconstructed tracks are discarded. For one-track events, the recoil proton or a pion is absent or below threshold. The requirement of three layers for the second track corresponds to a threshold of 600 MeV/c proton momentum and 200 MeV/c pion momentum. The MC simulation includes the interaction of protons, pions, and other hadrons from the neutrino interaction final state as they leave the nucleus. The models for these final state interactions are described, with references, in [8] and is in agreement with the number of tracks seen in SciFi. In the extreme case of zero final state interactions, the Monte Carlo simulation predicts 20% too many two-track events[24], most of which should have been one-track events, shown in Fig. 3.

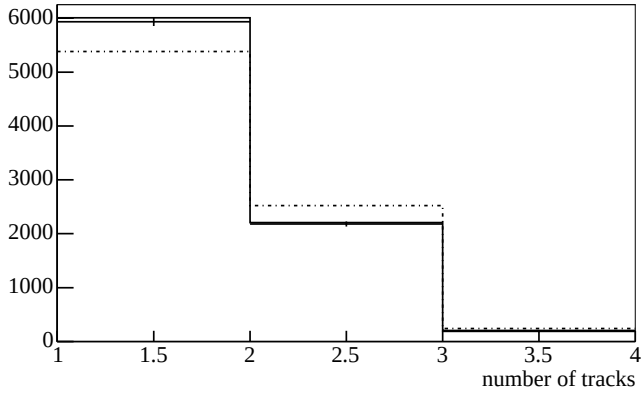

FIG. 3: K2K-I data showing the number of tracks for each event. The dotted [actually green] line shows the distribution with zero nuclear final state interactions, such as proton or pion rescattering. The solid histogram is the baseline MC. The statistical errors in the data are too small to see. [Rik: the no final state numbers are just estimates from the NuInt paper, while the data and solid line are the current official. If we choose to keep this plot, I will need to redo a MC study to obtain the correct numbers.]

For two-track events, we separate quasi-elastic from non quasi-elastic events. Quasi-elastic interactions are a two-particle scattering process; the measurement of the muon momentum and angle is sufficient information to predict the angle of the recoil proton. If the measured

second track agrees with this prediction within 25°, it is likely a QE event. If it disagrees, then it becomes a part of the non-QE sample. This is demonstrated in Fig. 4, where the inset diagram demonstrates the kine-

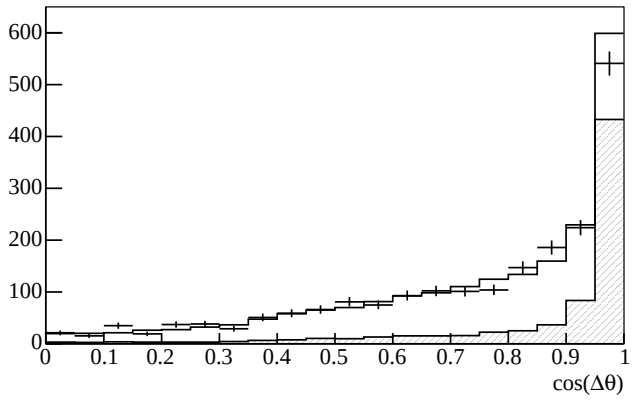

FIG. 4: The distribution of cos($\Delta\theta$), showing the difference between the predicted proton angle for QE events and the actual second track. The histogram shows the Monte Carlo prediction, while the hatched region shows the QE fraction. The vertical line is where we make the cut to separate QE from non-QE enhanced samples. The inset diagram shows the definition of $\Delta\theta$. [Rik will include the cut line and diagram in the next draft]

matic quantity $\Delta\theta$ = Predicted $\theta_{2ndTrack}$ - Measured $\theta_{2ndTrack}$ The quantity cos($\Delta\theta$) is plotted in this figure with the data and the baseline MC.

The value for this $\Delta\theta$ cut is chosen to give good separation between the QE and nonQE enhanced samples. We used the Monte Carlo simulation to estimate the efficiency for detecting the QE events, after all the cuts described above. Also we have estimated the purity of each sub-sample. These are shown in Tab. I. After these cuts, the total number of events in each sample is given in Tab. II.

	1-track	2-track		Total
		QE	nonQE	
K2K-I	35 (63)	5 (63)	2 (17)	42
K2K-IIa	38 (61)	5 (61)	2 (15)	45

TABLE I: Total reconstruction efficiency [%] for quasi-elastic interactions in each data set, the portion of efficiency from each sub-sample, and the QE purity of each sample (in parenthesis, [%]), estimated with MC simulation.

D. Muon momentum and angle distributions

An example of the muon momentum and muon angle distributions for the K2K-I data along with the Monte Carlo prediction are shown in Fig. 5 and Fig. 6.

	K2K-I		K2K-IIa	
	$Q^2_{rec} > 0.0$	$Q^2_{rec} > 0.2$	$Q^2_{rec} > 0.0$	$Q^2_{rec} > 0.2$
1 track	5933	2864	3623	1659
2 track QE	740	657	451	388
2 track nonQE	1441	789	893	478
Total	8114	4310	4967	2525

TABLE II: Number of events in three event samples and two data periods for the SciFi detector. Only events with reconstructed $Q^2 > 0.2$ (GeV/c)^2 are used for this M_A measurement, and are shown in separate columns and described in Sec. IV.

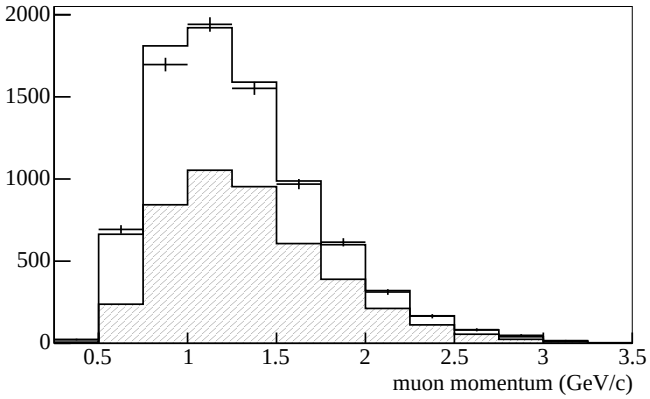

FIG. 5: Muon momentum distribution for all K2K-1 one-track and two-track events. The QE fraction, estimated from the MC simulation, is shown as the shaded region. The errors on the data are statistical only.

We observed a deficit of events whose muon is at angles near the direction of the beam compared to our Monte Carlo simulation; this is also discussed in [18]. The dis-

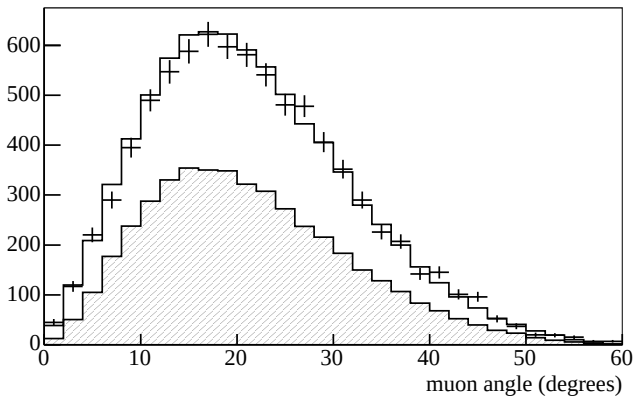

FIG. 6: Muon angle distribution for all K2K-I one-track and two-track events. The QE fraction, estimated from the MC simulation, is shown as the shaded region. The statistical errors on the data are smaller than the size of the dot.

crepancy was observed in all K2K near detectors, including SciFi, and is presumed to be from some aspect of the

neutrino interaction model. The analysis of data from the SciBar detector [12] indicated that most, if not all of this deficit is because there is too much coherent pion production in the MC. The SciBar data are consistent with zero charged-current coherent pion. Examples of the disagreement from SciFi data are shown in Fig. 7, with and without charged current coherent pion events.

IV. ANALYSIS

A. Calculating Q^2 and E_ν

The kinematics of the muon, the longest track in our events, are sufficient to estimate the energy of the neutrino E_ν^{rec} and the square of the momentum transfer Q^2_{rec}, if the interaction is quasi-elastic.

$$E_\nu^{rec} = \frac{(m_N+\epsilon_B)E_\mu - (2m_N\epsilon_B+\epsilon_B^2+m_\mu^2)/2}{m_N+\epsilon_B-E_\mu+p_\mu\cos\theta_\mu}, \quad (5)$$

$$Q^2_{rec} = -q^2 = -2E_\nu(E_\mu - p_\mu\cos\theta_\mu)+m_\mu^2. \quad (6)$$

Here, E_μ and p_μ are the energy and momentum of the muon, determined from the range, θ_μ is the angle relative to the incident neutrino direction, determined from the hits in the SciFi detector. Note that E_ν appears in the expression for Q^2_{rec}. The quantity ϵ_B = -27 MeV for oxygen is the effective binding energy parameter from the Fermi gas model. The masses m_N and m_μ are for the nucleon and the muon. The resolution for E_μ is 0.12 GeV, due mainly to the MRD segmentation, though the mean of the distribution is accurate to 1%. The resolution for θ_μ is about 1 degree, but there is a tail to this distribution for events with significant activity around the vertex. [Make sure of this statement.] The resulting value for E_ν resolution (for QE events) is 0.16 GeV and the resolution for Q^2 is 0.05 $(GeV/c)^2$ also with a tail coming from the measured angle. Finally, this formula assumes that the target neutron inside the nucleus is at rest, ignoring the nucleon momentum distribution for the event reconstruction. Fluctuations due to Fermi motion are about half the size of those due to detector and reconstruction effects, and contribute only a small amount to the reconstructed energy resolution.

It is important to note that these formulas are used for all events even though half the interactions are not quasi-elastic, because we do not identify the interaction mode on an event-by-event basis, nor is our beam at a fixed energy. The reconstructed E_ν and Q^2 are systematically off for these non quasi-elastic events: E_ν^{rec} is low by ∼0.4 GeV and Q^2_{rec} is low by ∼0.05 $(GeV/c)^2$. However, all events are treated the same way, both data and Monte Carlo events. Thus, the comparison of data and MC in the fit is valid, but the distributions of the reconstructed values are affected by the non quasi-elastic fraction.

B. Fit procedure

After calculating E_ν^{rec} and Q^2_{rec} for each event, the data are binned in five E_ν^{rec} bins: 0.5 to 1.0, 1.0 to 1.5, 1.5 to 2.0, 2.0 to 2.5, and greater than 2.5 GeV. The data are divided into Q^2 bins each of width 0.1 $(GeV/c)^2$. To ensure there are at least five events in each bin, the smaller number of events at higher Q^2 are combined into a single bin.

The expectation for the number of the events in each bin is computed for different values of the axial-vector mass and some systematic error parameters. Four free parameters describe the relative flux of incident neutrinos the different energy bins common to both data sets. There is also one parameter for the absolute normalization which is common to both data sets. This parameter is relative to the data/MC normalization calculated using the nominal parameters and M_A = 1.1 GeV. There is a scaling factor for the number of non-QE events to account for the uncertainty in the cross section relative to QE interactions. Two parameters describe a combination of interaction model and detector effects: a migration from two-track to one-track events accounts for errors in tracking efficiency and final state interactions, another parameter models the amount of proton rescattering and is primarily a migration beween the QE and nonQE enhanced two-track samples.

We perform a maximum likelihood fit to the data by minimizing the negative of the logarithm of the likelihood which is based on Poisson statistics for each bin. In our case we use the modified form given in the Review of Particle Physics [7]

$$-2\ln\lambda(\theta) = 2\sum_{i=1}^{N}[\nu_i(\theta) - n_i + n_i\ln(n_i/\nu_i(\theta))] \quad (7)$$

in which $\nu_i(\theta)$ and n_i are the predicted and observed values in the i-th bin for some values of the parameters θ. The minimum of this function follows a chi-square distribution and can be used to estimate the goodness of the fit.

The expectation for each reconstructed E_ν and Q^2 bin is computed as follows:

$$N_{total}(n_{track}, E_{rec}, Q^2_{rec}) = A\left[\mathrm{N_{QE}}(n_{track}, E_{rec}, Q^2_{rec}) + B\times \mathrm{N_{nonQE}}(n_{track}, E_{rec}, Q^2_{rec})\right]\times\Phi(E_{true}). \quad (8)$$

The free parameter A is the overall normalization and $\Phi(E)$ refers to five parameters that rescale the neutrino flux in each energy region, four of which are unconstrained in the fit, while the relative flux for energies from 1.0 GeV to 1.5 GeV is fixed at 1.0. The flux is reweighted based on the true energy of the MC events. The nonQE background is reweighted using the unconstrained parameter B, which is referred in the rest of this paper as the ratio nonQE/QE: the relative rewieghting of our default MC calculation. Because of the separation of

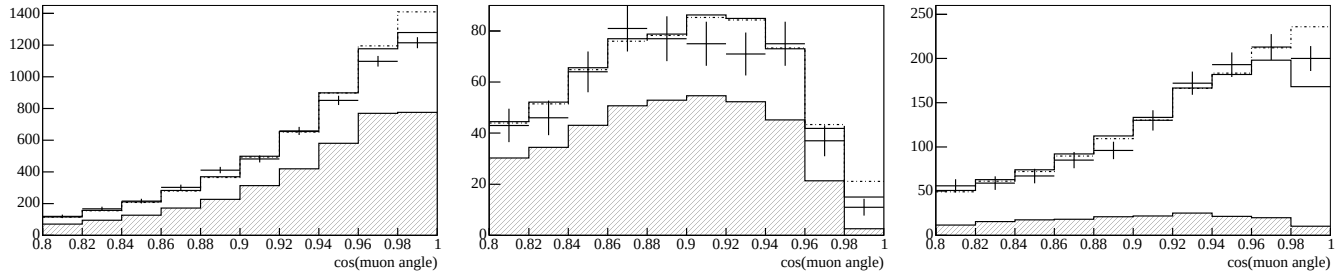

FIG. 7: Distribution of $\cos(\theta_\mu)$ for data and MC, showing the data at small angle, which is also the low Q^2. Left to right are the one-track, two-track QE enhanced, and two-track nonQE enhanced samples. The top line is with charged-current coherent pion, the second line without. The shaded region is the QE fraction, estimated from the MC simulation.

the two-track QE and non-QE samples, the nonQE/QE ratio will be constrained by the background and allow a fit for the QE axial-vector form factor.

In this expression, N_{QE} is based on a calculation of the quasi-elastic cross section with the free parameter M_A. This cross section is computed using the true energy and Q^2 and convoluted with the detailed shape of neutrino energy spectrum, flux(E), from the beam MC calculations.

$$N_{QE}(n_{track}, E_{rec}, Q^2_{rec}) = \sum_{Etrue,Q^2true}^{\text{all bins}} \Big[\text{flux}(E_{true}) \times d\sigma/dQ^2(E_{true}, Q^2_{true}, M_A) \times R(E_{true}, Q^2_{true}) \times M(E_{true}, Q^2_{true} \rightarrow n_{track}, E_{rec}, Q^2_{rec}) \Big]. \quad (9)$$

Cross section effects due to the nucleus, especially Pauli blocking, are included in the factor R.. Because the cross section is calculated using true kinematics, it must be modified to account for detector acceptance and resolution, as well as nuclear final state interactions, in order to obtain the expectation in different reconstructed E and Q^2 bins. This is done with a migration matrix M in the above equation where n_{track} refers to the one-track, two-track QE, and two-track non-QE samples. This matrix is computed directly from the Monte Carlo simulation. This result is then applied to the calculated cross section to determine the number of QE events in each reconstructed E_ν and Q^2 bin. In contrast, the shape of the non-QE background is taken directly from the Monte Carlo and already includes these effects.

The prediction for the neutrino flux, flux(E), for this fit is the one based on the hadron production parameterization. The combination of four flux reweighting factors $\Phi(E)$ and the overall normalization are unconstrained. The parameter M_A itself affects the total cross-section as a function of energy. In this way, we are fitting the shape of the Q^2_{rec} distribution separately *in each energy region*. This ensures that the axial mass measurement is not significantly biased by the normalization in any one energy bin.

Finally, the lowest Q^2_{rec} bins, events below 0.2 $(\text{GeV/c})^2$, are not included in the fit. The low Q^2 region is where there is the largest uncertainty due to the model for nuclear effects, especially Pauli blocking. This eliminates almost half the data, and the total number of events actually included in the fit is shown in the second column for each data set in Tab. II. Low Q^2_{rec} events are also events at low angle, shown by the $\cos(\theta)$ term in parenthesis in Eq. 6, and corresponds to the right-most two bins in the $\cos(\theta)$ histograms in Fig. 7 for neutrino energies around 1.0 GeV.

V. RESULTS AND DISCUSSION

A. Fit Results

We fit a large collection of E^{rec}_ν and Q^2_{rec} distributions: two data sets K2K-I and K2K-IIa, each with one-track, two-track QE, and two-track non-QE subsamples, a total of 241 bins. The Monte Carlo predictions for these data sets are computed separately using a MC sample that is more than 15 times larger than the data. The free parameters for the flux at each energy are common to both subsamples, as is the overall normalization factor, the non-QE/QE ratio and proton rescattering. There are separate 2-track to 1-track migration parameter for each sample, ten parameters in total.

The result of the combined fit is $M_A = 1.16 \pm 0.12$ GeV. The chisquare value for this fit is 260 for 231 degrees of freedom. The Q^2 distributions for the data and the MC simulation with the best fit M_A are shown in Fig. 8, with all five energy regions combined. The K2K-I and K2K-IIa samples are also fit separately. We obtain the values 1.12 ± 0.12 and 1.25 ± 0.18 respectively.

For the combined fit results, the best fit values for the free parameters in the fit are summarized in Tab. III. In the fit, there is a strong correlation between the normalization, nonQE/QE, and the two-track to one-track migration; this particular combination provides the best chisquare, but does not affect the fit value of M_A very much. The migration is expressed such that 0.90 means 10% of the two-track events in each E_{rec} and Q^2_{rec} bin should be moved to the corresponding one-track bin. For

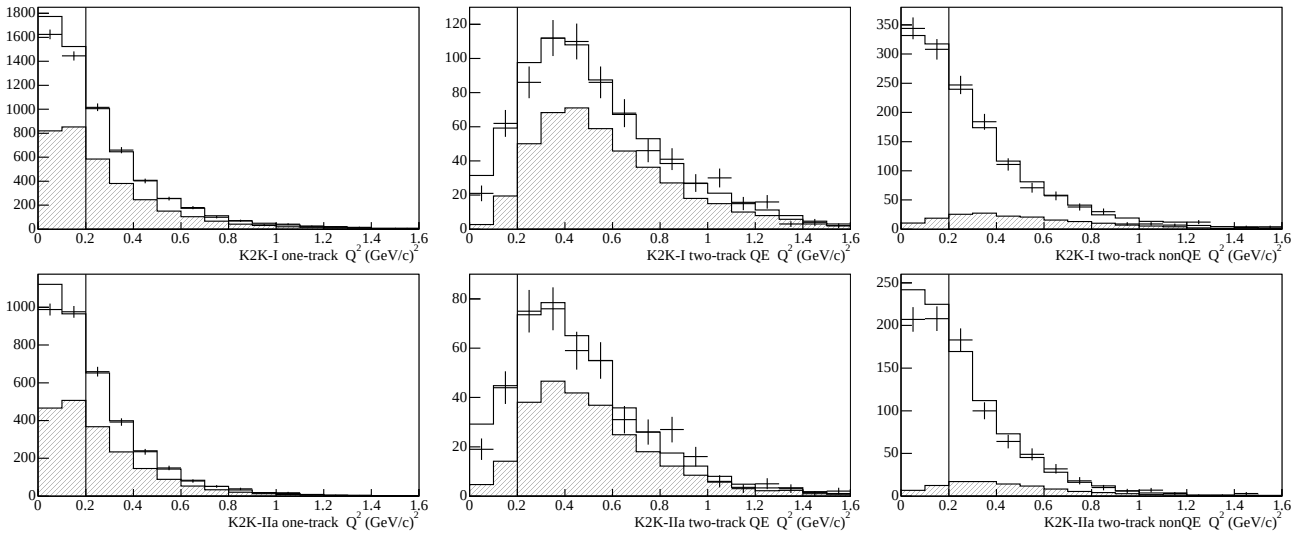

FIG. 8: The data and the best fit Q^2_{rec} distributions for K2K-1 data (top) and K2K-IIa data (bottom) for the 1-track, 2-track QE enhanced, and 2-track non-QE enhanced samples. The shaded region shows the QE fraction of each sample, estimated from the MC. The contribution from each energy region is summed for each plot. The lowest two data points in each plot are not included in the fit.

parameter	fit value	error
M_A	1.16	0.09
Φ(0.5 to 1.0 GeV)	0.93	0.26
Φ(1.0 to 1.5 GeV)	1.00	fixed
Φ(1.5 to 2.0 GeV)	0.81	0.09
Φ(2.0 to 2.5 GeV)	0.94	0.08
Φ(> 2.5 GeV)	1.11	0.11
Normalization	0.94	0.09
nonQE/QE	1.39	0.17
K2K-I 2tk → 1tk	0.90	0.25
K2K-IIa 2tk → 1tk	0.89	0.32
Proton Rescattering	0.90	0.08

TABLE III: Best fit values for the parameters in the fit. The errors given are from the fit only. The error for M_A rises to 0.12 when the other systematic effects are included

example, fixing the 2-track to 1-track migration to its nominal value yields nonQE/QE = 1.07 and normalization = 1.06, but M_A only shifts to 1.19 GeV and the chisquare rises to 276 for 233 degrees of freedom.

B. Consistency checks

A test for consistency is to vary the low Q^2 cut and compare the results.. In Fig. 9, the best fit M_A is shown with different minimum Q^2_{rec}. The error bars include an estimate of statistical errors only, however the data points themselves are correlated. The extra error bar shows the total error. When no cut is applied (and no coherent pion), the fit value is $M_A = 1.24 \pm 0.12$, where the statistical error is less, but a large systematic error of $\pm$ 0.07 is assigned due to uncertainty in the amount of Pauli Blocking.

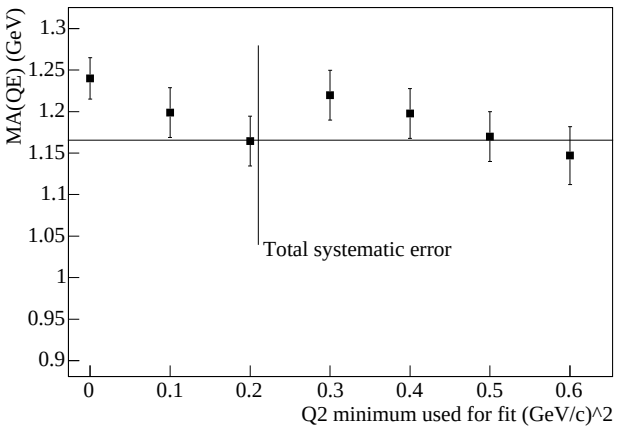

FIG. 9: Fit values obtained for different values of the low Q^2 cut. Only statistical errors are shown. The horizontal line is the combined best fit. The vertical line is the systematic errors.

A second check is to consider the fit values for the Q^2 distribution *at each energy*, shown in Fig. 10. This uses the best fit values for the flux for all energies except the one being tested while the chisquare, and therefore the shape fit, is computed only for the energy bins in question. This is necessary because of the significant migration from true energy (where the flux parameter is applied) to reconstructed energy used in the fit. There are different systematic effects, and this result should not be considered a measurement, but rather a consistency

test. However results for each energy are also consistent with the combined result.

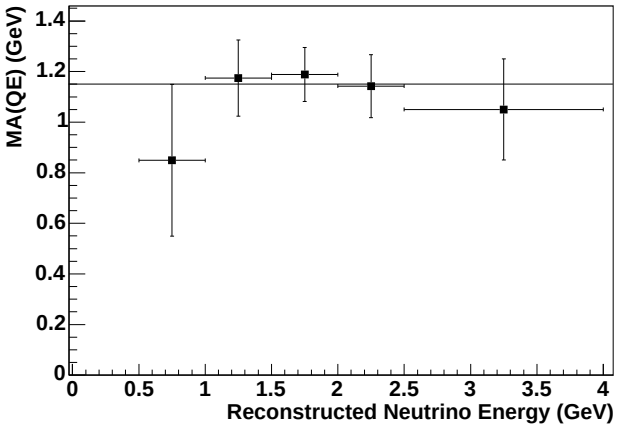

FIG. 10: Fit values obtained separately from the shape of the Q^2 distribution for each neutrino energy. The horizontal line indicates the combined best fit value.

C. Systematic uncertainties

The largest contributions to the systematic error, summarized in Tab. IV, are the uncertainty in the muon momentum scale, and the normalization and uncertainty in the flux for each energy region. Other, smaller contributions include the shape of the non-QE background, the non-QE/QE ratio, and the two-track to one-track migration. A final, interesting source of uncertainty comes from nuclear effects, though it contributes only a small amount to this analysis. The statistical error is estimated by setting all the other parameters in the fit to their best fit values and deterimine the resulting error in M_A, though there is a further statistical effect in the normalization parameter.

Sources of uncertainty	Error in MA
Energy Scale	0.07
Relative Flux and normalization	0.06
MA 1-π	0.03
nonQE/QE	0.03
Statistics	0.03
Total	0.12

TABLE IV: The calculation of the total error. Errors smaller than 0.03 are not listed The total value takes into account the correlations among those errors that are parameters in the M_A fit; the others are added to that total in quadrature.

1. Muon momentum scale

The muon momentum appears directly, and indirectly via E_ν, in the calculation of the value of Q^2 for each event. The uncertain absolute scale for this momentum, as modeled in the detector Monte Carlo simulation, will cause the MC prediction for the shape of the Q^2 distribution to be more or less compressed. As an example, a $\pm$ 1% error in the momentum scale gives a $\mp$ 0.05 error in the fit value for M_A. Approximately $\mp$ 0.01 of this error can be attributed to shifting a small number of events up or down one E_ν^{rec} bin. The other $\mp$ 0.04 is from the calculation of the reconstructed Q^2 itself. The central value for the muon momentum scale is determined from the spectrum fit analysis, described in Sec. III and reference[18], while the error from that analysis is propagated to the M_A analysis as described below.

Because the muon momentum is measured using its range in the detector, the uncertainty for the overall momentum may come from any of the pieces of the detector. In this analysis, we model this uncertainty by assigning it to two pieces. The first is the uncertainty in the density of the lead-glass detector and therefore the energy loss experienced by the muon passing through it. The second piece is a scaling factor for part of the muon momentum calculated from the range in the MRD detector. For both pieces, we determine the central value of the momentum shift and the error from the neutrino data.

The density of the lead glass, which is incorporated into the geometry description in our Monte Carlo simulation, is determined from a beam test and is uncertain by 5%. We have modeled the effect of this uncertainty and made a reweighting table that modifies the MC p_μ and θ_μ distribution. This uncertainty could give rise to a 2% error in the total momentum for a typical K2K-I event. In the spectrum analysis used for the oscillation measurement, this is a parameter in the fit and good agreement with the data is found with a value that is 0.98 $\pm$ 0.013 times the density obtained from the beam test; the neutrino data provides the stronger constraint. This central value is used in the M_A analysis.

Likewise, we measure a shift in the muon momentum scale for in the Muon Range Detector (MRD) of 0.976 $\pm$ 0.007 using the spectrum fit procedure. When the K2K-I and K2K-IIa data are fit separately, we obtain a consistent result for this parameter, despite the presence of the lead glass detector in the former. This is assigned as an error for the MRD portion of the muon range, but it actually arises from a combination of factors including the material assay for the MRD and SciFi (about 1%), the simulation of muon energy loss in GEANT [25] (about 1%) and the uncertainty in the intrinsic muon momentum from the neutrino interaction MC (about 0.5%).. Again, we find the neutrino data produces a good central value and a tighter constraint than taking the individual errors in quadrature. Though these errors actually come from all portions of the muon track, we find no significant difference in the analysis if this factor is applied to

the whole track momentum, instead of the MRD portion only.

Because the M_A fit and the spectrum fit use the same neutrino data, it is possible that the uncertain value for M_A itself is affecting the fit values for the MRD muon momentum scale when that value is obtained from the spectrum fit. Our default Monte Carlo assumes M_A = 1.1 GeV. An uncertainty in this value of ± 0.20 GeV corresponds to an error of ± 0.01 in the fit value of the momentum scale. This is taken as an additional uncertainty when this parameter is used to determine M_A. Also, there is a correlation between the lead-glass density error and the MRD momentum error. When all of these effects are combined, the resulting error in M_A is ± 0.07.

2. *Flux for each energy region and normalization*

A significant uncertainty arises because the relative neutrino flux for each energy region and the overall normalization parameters are unconstrained parameters in the fit. In this way we are fitting the shape the Q^2 distribution in each energy region separately, regardless of the errors in the incident neutrino flux. The contribution to the total error is estimated by fixing the other free parameters in the fit and reading the resulting error in M_A, which is from these parameters and statistics only.

The overall normalization contributes more to the error than the uncertain relative normalization. This is estimated by further constraining the relative flux so that only the normalization and M_A are free. The overall normalization is correlated with M_A because M_A affects both the relative size of and the shape of the QE cross-section. Different combinations of MA and normalization will give a reasonable chisquare when compared with the data, and the error due to this parameter, more than the others, would be reduced with increased data statistics, even with no further constraints. This last result is confirmed using MC samples of various sizes as if they were data, to study the effect of statistics of the data sample.

We do have a constraint on the relative flux for each energy region from the neutrino oscillation measurement [18]. This measurement is done using data from all the near detectors, not just SciFi. This information is not completely independent of this analysis because it shares some of the same data set, but a different analysis technique, and several other data sets from the other near detectors. We get a consistent result $M_A = 1.13 \pm 0.12$ when this constraint is used.

3. *nonQE/QE parameter and two-track to one-track migration*

The nonQE/QE scaling ratio is also a free parameter in the axial-mass fit. There is no constraint on this parameter for this analysis, though other estimates find that it is uncertain by 5 to 10% [18]. The two-track to one-track migration parameter is highly correlated with nonQE/QE, and when these two are combined, they contribute a total error of 0.03 to the fit value of M_A. As before, this is obtained by fixing all the other parameters such that the resulting error in M_A is the combination of these and the statistical error only.

[As described in my e-mail, the nonQE/QE parameter is an effective parameter. Following Sofia Andringa's suggestions, Rik will try to pick apart the contributions to nonQE/QE, to see what physics information can be obtained. If this is successful, it can be reported here. This analysis is not complete yet.]

4. *Non quasi-elastic background shape*

Single pion events from the production and decay of the Δ and other resonances in the nucleus are the largest background to the QE samples in this analysis. These events are described by a calculation that includes a similar axial mass parameter which affects the shape of the Q^2 distribution. If the value used to model the single pion background is different, that will affect the fit value obtained for the quasi-elastic events. Our calculation takes $M_A^{1\pi} = 1.1 \pm 0.1$ GeV. This contributes an uncertainty of ± 0.03 to result for M_A^{QE}, and is estimated by generating a second complete MC sample with $M_A^{1\pi} = 1.2$ GeV.

Other contributions to the nonQE background are deep inelastic scattering and coherent pion production. For the former, we have evaluated the uncertainty by removing the Bodek-Yang correction, and find no effect. We also consider the case where charged-current coherent pion events are produced which has only +0.01 GeV effect for the $Q^2 > 0.2$ cut used in the standard analysis, but increases the fit value by 0.10 GeV when we fit the entire Q^2 range.

5. *Nuclear effects*

Other interesting sources of uncertainty are the effects of the nucleus on the cross section and the Q^2 distribution, primarily from the nucleon momentum distribution. The effects are small relative to the other uncertainties described above because the minimum Q^2_{rec} cut eliminates the data where these errors are most significant. These effects will be of interest for future precision experiments and as models of neutrino-nucleus interactions become more sophisticated. We present a description of these effects for the uniform Fermi gas model, in this case from the calculation in [26, 27]. The three effects are described below and summarized in Fig. 11 for a 1.0 GeV neutrino. It is the ratio in this figure that is the basis for $R(E,Q^2)$ in Eq. 8.

The main uncertainty is the amount of Pauli Blocking that should be applied both to the quasi-elastic and also the single pion background. Within the context of the

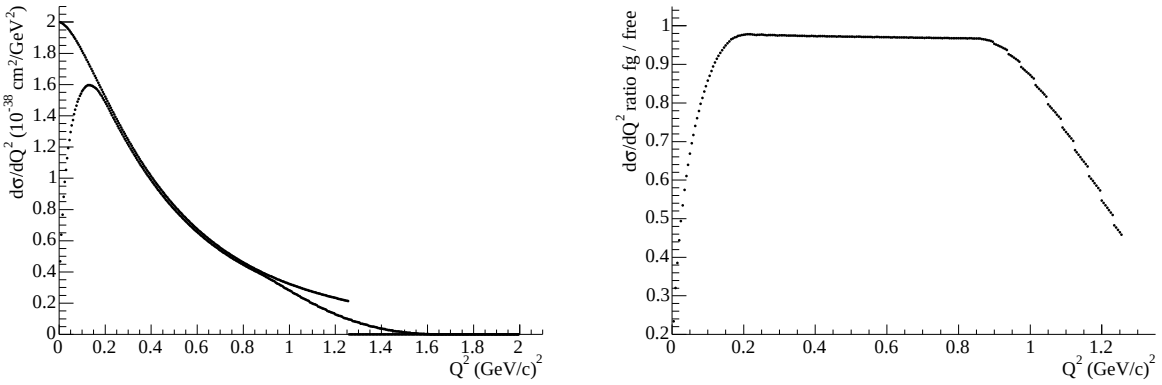

FIG. 11: Effect of the nucleon momentum on the shape of the Q^2 distribution. The comparison is between the free nucleon and a uniform Fermi gas model. The effect of Pauli blocking is seen at low Q^2, the tail of the momentum distribution at high Q^2, an overall suppression, and a slight change in the slope in the middle region. The calculated quasi-elastic cross sections for 1.0 GeV neutrinos on oxygen are on the left, and the ratio (Fermi gas)/ (free neutron).

Fermi gas model, this can be estimated by assuming a different k_f: 215 and 235 in addition to the default value of 225 GeV/c. The effects of this uncertainty on M_A do not appear with the $Q^2 > 0.2$ requirement used in this analysis, but are as much as 5% at the lowest Q^2.

At upper end of the Q^2 distribution, the quasi-elasitic cross section has a kinematic cut off whose location depends on the incident neutrino energy. The momentum distribution in a nucleus smears this step, giving a tail to the distribution. These high Q^2 interactions produce muons that do not reach the MRD because they are at high angle or their momentum is too low, so this has no effect on the present analysis.

The momentum distribution will modify the shape of the Q^2 distribution through the middle region between the two effects described in the preceeding paragraphs. The slope of the middle region in the second plot in Fig. 11 is approximately 0.017 $(\mathrm{GeV/c})^{-2}$. There is also an overall suppression of the cross section of 2%. The uncertainty represented by the change in slope can be propagated to the M_A analysis by modifying $R(E,Q^2)$ in the fit. The resulting uncertainty in M_A is ± 0.01, negligible compared to the other uncertainties in this analysis.

A final uncertainty from the nuclear model is the nucleon interaction energy. For our Fermi gas model, this takes the form of an effective binding energy -27 $\pm$ 3 MeV, and is the energy given up to the recoil proton from the nucleus. This affects the outgoing muon momentum and would contribute $\pm$ 0.02 error to M_A, but this is naturally included by the free energy scale parameter in this analysis.

These uncertainties are also used to estimate the effect of the 21.7% aluminum that makes up the fiducial mass. The neutrino-aluminum interactions are taken to have the same cross section per nucleon and the same kinematics as for oxygen. A higher k_f appropriate for aluminum only has an effect in the Pauli blocked region and the increased effective binding energy has an effect equivalent to a shift in p_μ of about 3 MeV for this fraction of the events, and thus is negligible for the whole sample.

D. Effect of the new form factors

The basic method used to measure the axial vector mass here is the same as for previous measurements, listed in Tab. V, but since that time there have been improved measurements for the shape of the vector form factors from electron scattering experiments. Changing the shape of the contribution of the vector form factors affects the fit shape of the axial-vector form factor. We continue to assume F_A has a dipole form; future high-precision neutrino experiments may be sensitive to subtle differences from a F_A dipole shape. Our results are extracted using these updated parameterizations, but in order to allow comparison with the previous results, we have repeated the analysis with the same modified dipole approximations used by [4–6] who follow Olsson *et al.* [34]. We find that these old parameterizations produce a value that is 1.20, roughly 0.04 higher. When only a pure dipole is used, the fit value is 1.23 MeV.

Our results assume a parameterization of the vector form factors according to Bosted [2]. We have evaluated one other parameterization [3] and found the M_A result differs by only 0.01 GeV. This is true even considering the discrepancy between the polarization transfer measurement and the Rosenbluth separation measurement, described in [3] with further references. [Add the most important references directly to this paper?]. For our analysis, we use the parameterization of G_E^N given by [35].

Experiment	Pub. Date	Target	Method	MA	Error	comment
ANL [6]	1982	D	12' Bubble Chamber	1.00	± 0.05	
FNAL [5]	1983	D	15' Bubble Chamber	1.05	+0.12 - 0.16	
BNL [4]	1990	D	7' Bubble Chamber	1.07	+0.040 -0.045	
CERN [28]	1977	CF_3Br	GGM Bubble Chamber	0.94	± 0.17	
CERN [29]	1979	CF_3Br, C_3H_8	GGM Bubble Chamber	0.94	± 0.05	
SKAT [30]	1990	CF_3Br	Bubble Chamber	1.05	± 0.14	(ν)
SKAT [30]	1990	CF_3Br	Bubble Chamber	0.79	± 0.20	(ν-bar)
BNL [31]	1969	Fe	Segmented Tracker	1.05	± 0.20	
BNL [32]	1987	HC, Al	Segmented Tracker	1.06	± 0.05	elastic scattering
BNL [33]	1988	HC, Al	Segmented Tracker	1.09	± 0.04	(ν-bar)
K2K SciFi	this expt.	H_2O, Al	Segmented Tracker	1.23	± 0.12	dipole form factors

TABLE V: Results from other experiments, grouped first by target nucleus, then by publication date. Where separate values are given for M_A extracted from the shape of $d\sigma/dQ^2$ only, that is the value included in this table. All the data are for the neutrino quasi-elastic reaction (ν n $\rightarrow \mu^-$ p) except for two which also took data with anti-neutrino (ν-bar p $\rightarrow \mu^+$ n), one of which studied neutral current (elastic) scattering, noted in the table. For better comparison with other experiments, the K2K SciFi result is the one analyzed with dipole vector form factors.

E. Comparison with other experiments

This is the first measurment of the axial vector mass using neutrino interactions with oxygen targets, but there have been many previous measurements with a variety of other target nuclei. The experiments in Tab. V have hundreds or thousands of events from neutrino or anti-neutrinos with energies of a few GeV. The systematic errors they report are dominated by uncertainties in the neutrino flux, calculation of nuclear effects, and subtraction of non-quasielastic backgrounds.

One problem with comparing the results in Tab. V is that the older analyses used not only different assumptions about the vector form factors, but also different backgrounds and other physical constants such as $F_A(q^2{=}0)$ The results given here are the published results, however the authors of [3] have made some effort to reproduce and then update all of the analysis assumptions for a selection of these experiments.

VI. CONCLUSION

We have made the first measurement of axial vector form factor using neutrino interactions on an oxygen target. We find an axial vector mass $M_A = 1.16 \pm 0.12$ GeV/c^2 gives the best agreement with the data, if we assume a dipole form for F_A. This analysis includes the updated (non-dipole) vector form factors obtained from electron scattering experiments. In order to better compare with previous experiments, an alternate result using only pure dipole vector form factors is $M_A = 1.23 \pm 0.12$ GeV/c^2. We have also studied the details of the nucleon momentum distribution for oxygen on this analysis and find only a small effect on the shape of the Q^2 distribution for $Q^2 > 0.2$.

Acknowledgments

Acknowledgments not yet written.

[1] C. L. Smith, Phys. Lett. C **3C** (1972).
[2] P. E. Bosted, Phys. Rev. C **51**, 409 (1995).
[3] H. Budd, A. Bodek, and J. Arrington, hep-ex/0308005 (2002).
[4] T. Kitagaki et al., Phys. Rev. D **42**, 1331 (1990).
[5] T. Kitagaki et al., Phys. Rev. D **28**, 436 (1983).
[6] K. Miller et al., Phys. Rev. D **26**, 537 (1982).
[7] S. Eidelman et al., Phys. Lett. B **592** (2004), URL `http://pdg.lbl.gov`.
[8] Y. Hayato, Nucl. Phys. B Proc. Supp. **112**, 171 (2002).
[9] D. Rein and L. Seghal, Ann. Phys. **133**, 79 (1981).
[10] M. Gluck, E. Reya, and A. Vogt, Z. Phys. C **67**, 433 (1995).
[11] A. Bodek and U. K. Yang, Nucl. Phys. B Proc. Supp. **112**, 70 (2002).
[12] M. Hasegawa et al., Submitted to Phys. Rev. Lett. (2005), hep-ex/0506008.
[13] D. Rein and L. Seghal, Nucl. Phys. B **223**, 29 (1983).
[14] J. Marteau, Eur. Phys. J. A **5**, 183 (1999).
[15] J. Marteau, J. Delorme, and M. Ericson, Nucl. Instrum. Methods A **451**, 76 (2000).
[16] S. H. Ahn et al., Phys. Lett. B **511**, 178 (2001).

[17] M. H. Ahn et al., Physical Review Letters **90**, 041801 (2003).
[18] E. Aliu et al., Phys. Rev. Lett. **94**, 081802 (2005).
[19] S. Fukuda et al., Nucl. Instrum. Methods A **501**, 418 (2003).
[20] K. Nitta et al., Nucl. Instrum. Methods A **535**, 147 (2004).
[21] K2K MRD Group, T. Ishii, et al., Nucl. Instrum. Methods A **482**, 244 (2002).
[22] A. Suzuki et al., Nucl. Instrum. Methods A **453**, 165 (2000).
[23] B. J. Kim et al., Nucl. Instrum. Methods A **497**, 450 (2003).
[24] C. Walter, Nucl. Phys. B Proc. Supp. **112**, 140 (2002).
[25] R. Brun et al., CERN DD/EE/84-1 (1987).
[26] H. Nakamura and R. Seki, Nucl. Phys. B Proc. Supp. **112** (2002).
[27] H. Nakamura and R. Seki, Nucl. Phys. B Proc. Supp. (2002), proc. NuInt02, Irvine, in press.
[28] S. Boneti et al., Nuovo Cimento A **38**, 260 (1977).
[29] N. Armenise et al., Nucl. Phys. B **152**, 365 (1979).
[30] J. Brunner et al., Z. Phys. C **45**, 551 (1990).
[31] R. Kustom et al., Phys. Rev. Lett. **22**, 1014 (1969).
[32] L. Ahrens et al., Phys. Rev. D **35**, 785 (1987).
[33] L. Ahrens et al., Phys. Lett. B **202**, 284 (1988).
[34] M. G. Olsson, E. T. Osypowski, and E. H. Monsay, Phys. Rev. D **17**, 2938 (1978).
[35] S. Galster et al., Nucl. Phys. B **32**, 221 (1971).